A TWO-DIMENSIONAL MODEL TO PREDICT WEB-TO-ROLLER TRACTION AT SMALL WRAP ANGLES

by

B. S. Rice[1] and R. F. Gans[2]
Eastman Kodak Company[1]
University of Rochester[2]
USA

ABSTRACT

We have studied the traction developed between a thin, flexible web and a rotating circumferentially grooved cylindrical roller. The traction model developed by Rice and Gans [1] is inadequate for small wrap angles, because of the two-dimensional nature of the airflow in the entrance nip. We develop a new two-dimensional analytic model that couples air film pressure, web deflection, and asperity contact to predict traction for circumferentially grooved rollers with arbitrary wrap angles. The entrance effects are incorporated into our new traction model by adapting the squeeze film concept using the distance from the entrance as a surrogate for time. We introduce dimensionless groups that the roller designer can use to quantitatively assess the interactions of process variables (e.g., speed and tension) with design variables (e.g., groove depth, groove pitch, roughness, etc.) over the full range of practical wrap angles. Finally, we verify this model experimentally on a series of fourteen rollers and nineteen webs. The roller surfaces range from non-grooved to circumferentially grooved.

NOMENCLATURE

Greek:

α	combined asperity engagement height
α_r	roller asperity engagement height
α_w	web asperity engagement height
γ	effective venting
δ	function used in defining web roller spacing without air entrainment
Δt	time required for web to travel from h_i to h_f
ΔT	T_{high0}-T_{low0}
θ	roller-wrap angle
θ^*	dimensionless grouping that defines high wrap
θ_{eff}	effective roller-wrap angle
μ	air viscosity

ν	web Poisson's ratio
ρ	mass density of the web

Roman:

A_{xc}	cross-sectional area
B^*	dimensionless grouping that defines thin web
c	web thickness
D	flexural rigidity of the web
E	Young's modulus of elasticity for web
f	static coefficient of friction
f_e	effective coefficient of friction
F_c	web-to-roller contact force
F_T	web-to-roller contact force without air entrainment
G_{D}	groove depth
G_{Deff}	effective groove depth
G_{w}	groove width
h	web-to-roller clearance
h_{eff}	effective web-to-roller clearance during contact
h_f	final web-to-roller clearance
h_i	initial web-to-roller clearance
h^*	dimensionless grouping relating actual web-to-roller clearance to effective web-to-roller clearance
l	width of arbitrary cross section
L_F	land fraction
L_w	land width
N	number of grooves per meter
p	air pressure under web
P_a	steady-state air pressure under the web
P_c	contact pressure between web and roller
P^*	dimensionless grouping relating air pressure to web tension pressure
R	roller radius
R_{pm}	surface roughness parameter, average of the five highest peaks in the sample, measured from the mean plane
R_z	surface roughness parameter, difference between the average of the five highest peaks and the five lowest valleys in the sample, measured from the mean plane
t	time
T	web tension per unit width, $T = T_0 - c\rho V_w^2$
T_0	nominal web tension per unit width
T_{high}	high-side web tension per unit width, $T_{high} = T_{high0} - c\rho V_w^2$
T_{high0}	nominal high-side web tension per unit width
T_{low}	low-side web tension per unit width, $T_{low} = T_{low0} - c\rho V_w^2$
T_{low0}	nominal low-side web tension per unit width
V	transport velocity, $V = V_r + V_w$
V_r	roller-transport velocity
V_w	web-transport velocity
w	web displacement
W	bearing width
x	longitudinal spatial coordinate

y cross-width spatial coordinate
z spatial coordinate perpendicular to web

INTRODUCTION

We study the traction developed between a thin, flexible web and a rotating cylindrical roller with circumferential grooves, analytically and experimentally, in this paper. In most applications, web-to-roller traction is the key to successful use of rollers. The maximum average contact pressure between the web and roller is at zero speed. As the web and roller speeds increase from zero, the converging geometry of the inlet region of the web/roller interface acts as a wedge bearing, resulting in super-ambient air pressure between the web and roller. The increase in the magnitude of the super-ambient air pressure causes a corresponding decrease in contact pressure in order to maintain equilibrium.

Rice and Gans [1] developed a simple model for the reduction of web-to-roller traction as a result of air lubrication (hereafter referred to as the "1D model"). The 1D model predicts the "steady state" (far from the ends of the lubrication region) air pressure between the web and roller by judicious use of the foil-bearing concept. They demonstrated excellent correlation between model and experiment for both non-grooved and high-wrap circumferentially grooved rollers. The 1D model has proved invalid for low-wrap circumferentially grooved rollers, an important application. Many web-converting machines use air impingement dryers. This type of dryer uses low-wrap backside rollers with 10 to 15° of wrap and front-side air impingement to dry a coating applied to the web. Hourticolon *et al.* [2] discusses this type of dryer.

Grooves allow the airflow to be two-dimensional (2D) on a macroscopic level, which causes the length of the nominal contact zone to be reduced. The 1D model assumes that the constant gap/pressure region (nominal contact zone), as predicted by the foil bearing, is unchanged by the presence of grooves. Grooves in the 1D model only modify the constant gap pressure by creating a larger effective web-to-roller clearance.

Modeling web-to-roller traction of low-wrap circumferentially grooved rollers is currently done using finite difference (FD) fluid/structure interaction (FSI) codes (e.g., [3]). FSI codes represent progress in understanding the web-to-roller traction problem for low-wrap cases, but the roller designer is still left with a difficult task. The investment of time and education needed to implement FSI codes is large. In addition, FSI codes require considerable computer resources. Depending on the size of the mesh required, a 2D FSI code may take from several hours to several weeks to run on today's computers (2 GHz processing speed). Therefore, the roller designer typically resorts to trial-and-error experimental techniques to design a low-wrap roller with adequate traction.

This trial-and-error experimental technique is both costly and time consuming. Thus, a simple analytic model for design of low-wrap rollers with adequate traction is needed. In this paper, we seek to identify and isolate the important parameters for the typical web-to-roller traction problem. Our goal is to develop a simple model that can be used to design rollers with adequate traction for the desired operating conditions. To this end we "re-derive" a capstan equation for non-grooved or circumferentially grooved rollers for arbitrary wrap angles, an extension of the work reported in [1].

Contact between the web and roller is only possible after the air has been squeezed from the lands into the grooves. This paper is devoted to the quantification of this idea. We will show there is a loss of wrap angle (contact) associated with this effect. The 1D model neglects this very important effect. We will model the entrance region, allowing

the distance to reach the "steady state" to be assessed. This is done adapting the squeeze film concept using the distance from the entrance as a surrogate for time.

Smith and Von Berhren [4], Keshavan and Wickert [5], Ducotey and Good [6,7], and Hashimoto [8] all used the squeeze film equation to account for side flow for non-grooved rollers or web winding. The squeeze film equation [9] is:

$$\Delta t = \frac{\mu \cdot W^2}{2 \cdot T / R} \cdot \left[\frac{1}{{h_f}^2} - \frac{1}{{h_i}^2} \right], \qquad \{1\}$$

where W denotes the bearing width, h_i denotes the initial film gap, h_f denotes the final film gap, Δt denotes the time for the web to move from h_i to h_f, μ denotes the dynamic viscosity of air, $T = T_0 - c\rho V_w^2$, and T_0 denotes the nominal web tension-per-unit width.

In this paper, we will derive a squeeze film equation that is valid for circumferentially grooved rollers. This simple squeeze film equation will correct the 1D model to account for 2D airflow in the entrance nip, reducing the nominal wrap angle to an effective wrap angle (θ_{eff}). Our new model is valid for arbitrary wrap angles for circumferentially grooved rollers with flat lands. We will show that the time required to squeeze the air from the lands into the grooves is directly related to web/roller surface roughness, land width, and web tension. The squeeze film analysis will also allow us to quantify the term "high wrap."

2D ANALYTIC TRACTION MODEL

Web/Roller System

A schematic of a web roller system with the appropriate coordinate system is shown in Fig. 1. Web deflection is in the z direction and is labeled w. The parameter δ is a function of x and y and represents the web-to-roller spacing without air entrainment. The air gap h is equal to $w+\delta$. Later in the paper, we will exploit the symmetry boundaries shown in Fig. 1 in our squeeze film analysis.

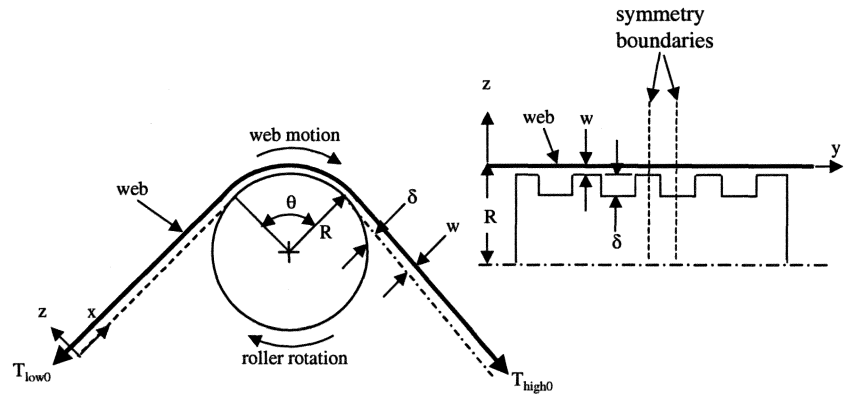

Fig. 1. - Roller/web schematic and coordinate system.

Physical Explanation of the Entrance Effects

The nominal wrap angle is shown in Fig. 1. The nominal wrap angle is based on the web path geometry assuming that the web is perfectly flexible (in the circumferential direction). In the 1D model, we assumed there was web-to-roller contact over the entire θ. For grooved rollers, there is a portion of θ (toward the entrance nip) where contact is not possible. No contact is possible until the air has been squeezed from the lands into the grooves. This takes a finite amount of time. The greater this time, the greater the portion of θ where contact cannot take place.

In the converging geometry of the entrance nip, the air pressure (as predicted by lubrication theory) is higher over the lands than the grooves because of the smaller air gap over the lands. The pressure in a groove starts from atmospheric pressure. The air above a land squeezes into its two adjacent grooves and flows along these grooves toward the entrance nip. This requires a positive pressure gradient from the entrance nip to the point of contact on the roller [10]. The pressure in the grooves builds to its final steady-state air pressure just prior to contact. Immediately at contact, the air pressure above the land must become equal to the air pressure in the groove.

There is no "compliance" in our idealized system. The fluid is incompressible, the web is rigid in the cross-width direction, and the web/roller asperities are rigid. Because the air is supposed to be incompressible, airflow from the lands would require that the air volume between the web and roller over the lands to decrease in order to conserve mass. This is only possible after contact if the web and/or asperities are compliant. Thus at contact, all pressure-driven airflow stops and the air pressure above the land and the groove equalizes. Because the air volume in the groove is much larger than the air volume over the land, the steady-state air pressure after contact is simply the air pressure in the groove just prior to contact [10].

The 1D model worked well for the high-wrap grooved rollers studied in [1] because the grooved rollers studied all had a fine groove pitch for which the time required to squeeze the air from the land is small, and the loss of contact in the entrance nip is insignificant. This is not true for coarse-pitch grooved rollers for which the loss of contact in the entrance nip can be significant.

Squeeze film Equation Used to Predict a Loss of Wrap Angle

We suppose that: web tension is uniform in the cross-width (y) direction; the system is infinitely wide (neglect edge effects); the fluid incompressible; the web is a membrane in the circumferential (x) direction and rigid in the cross-width (y) direction; the roller is grooved; the lands are flat; the web and roller are rough; airflow is possible during web-to-roller contact through the voids in the mating surfaces and along the grooves; the contact and air pressure act over the same area ($R\theta W$); the asperities are infinitely stiff; and the web has mass. We suppose that the steady-state air pressure (P_a) between the web and roller during contact is given by [1]:

$$P_a = \frac{3.094\mu V}{R}\left(\frac{R}{h_{eff}}\right)^{3/2}, \qquad \{2\}$$

where h_{eff} is calculated as shown in Rice and Gans [1]. We further suppose that the presence of grooves reduces the length of the contact zone from its nominal value.

The "standard" 1D squeeze film equation, Esq. 1, determines how long it takes a rigid, massless surface under a constant load to move a certain distance perpendicular to that load. The air squeezed out between the mating surfaces discharges to atmospheric pressure. We develop a modification to this equation to analyze airflow from the lands

into the grooves. We include the mass of the web and the details of the change in groove pressure. A schematic of a web roller system is shown in Fig. 1. An enlargement of the area of interest for the squeeze film analysis is shown in Fig. 2.

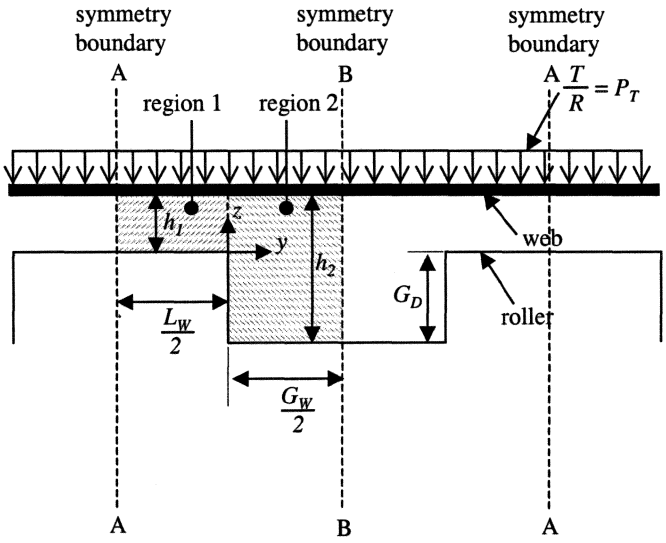

Fig. 2. - Schematic of a squeeze model for a grooved roller.

The ratio h_2/h_1 is much greater than 1. Therefore, the groove pressure (in region 2) is much lower than the average pressure over the land (in region 1). This will cause a net flow of air from the land areas to the groove areas. We assume that P_2 can vary with time but is constant in the y-z plane. (Rice [10] studied the case where P_2 can vary in the y-z plane.) The flow between adjacent lands is restricted by the symmetric nature of the problem. Air cannot flow across the symmetry boundaries labeled A-A and B-B in Fig. 2. There is no net flux from one groove to the next, or from one land to the next. This follows from neglect of edge effects. Similar arguments were made in the derivation of the foil bearing equation and the 1D traction model [1].

Ducotey and Good [6] showed experimentally that the air gap between a non-grooved roller and a flexible web can be predicted by a linear combination of the foil bearing equation and a 1D squeeze film equation. The foil bearing equation is used to predict the air gap in the constant gap/pressure region. The change in the "constant gap" region (in the circumferential direction) is predicted by a 1D (in the cross-stream direction) squeeze film analysis. We adopt their idea to model flow from land to groove. This requires that the system shown in Fig. 2 be infinite perpendicular to the page, requiring the aspect ratio of land width to wrap length to be much less than unity. A typical coarse-pitch, low-wrap roller case (Table 1, rollers 5 and 6 at 10° of wrap) has an aspect ratio of

$$\text{aspect ratio} = \frac{L_W}{R\theta} = \frac{650x10^{-6}}{(0.035)\cdot(0.174)} \approx 0.1.$$

This aspect ratio is smaller than that used in [6], and we are confident in using the 1D squeeze film to model flow from land to the groove.

We assume the flux across sections A-A and B-B to be zero. A free body diagram (FBD) is shown in Fig. 3.

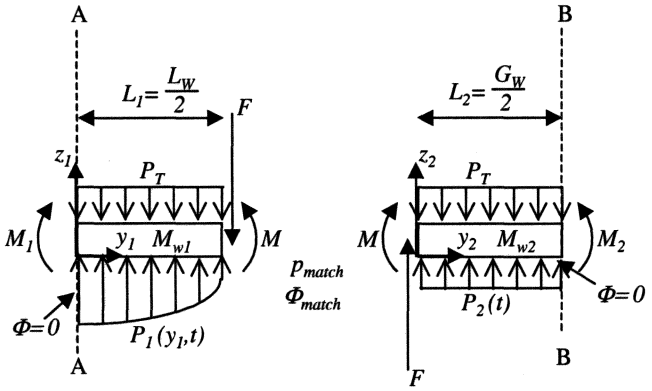

FBD I (per unit width) FBD II (per unit width)

Fig. 3. - Free-body diagrams of the web in the land and groove areas.

Newton's second Law in FBD I yields:

$$\int_0^{L_1} P_1(y_1,t)dy_1 - P_T L_1 - F = M_{w1}\frac{d^2h}{dt^2}. \qquad \{3\}$$

Newton's second Law in FBD II yields:

$$(P_2(t) - P_T)L_2 + F = M_{w2}\frac{d^2h}{dt^2}. \qquad \{4\}$$

The standard Reynolds equation for squeeze films [9] gives:

$$\frac{\partial^2 P_1(y_1,t)}{\partial y_1^2} = \frac{12\mu}{h_1^3}\frac{\partial h}{\partial t}. \qquad \{5\}$$

We have 3 equations and 4 unknowns: $P_1(y_1,t)$, $P_2(t)$, $h(t)$, and $F(t)$. We require a fourth equation. We argue that $P_2 = P_a$ is that equation. The pressure in the grooves starts off at atmospheric pressure. It builds to the steady-state air pressure (P_a) given by Eq. 2 just prior to contact. The initial pressure above the lands will be much higher than that in the groove because of the smaller air gap [10]. This pressure differential will drive air from the lands into the grooves. The grooves, if deep enough, will look like an infinite sink at atmospheric pressure. If the grooves are not deep enough, their pressure will be above atmospheric pressure but much lower than the initial air pressure over the lands. Thus, we suppose that the groove pressure is equal to a constant, P_a, given by Eq. 2.

We further suppose that the web mass is negligible, and the initial height of the web above the lands is denoted by h_i. These assumptions lead to the following ordinary differential equation for h:

$$\frac{4\mu L_1^3}{h^3}\frac{dh}{dt} = (P_a - P_T)(L_1 + L_2)\cdot \qquad \{6\}$$

Eq. 9 can be solved analytically for the time required for the web to move from h_i to a given spacing h.

$$\Delta t = \frac{2\mu \cdot L_1^3}{(P_T - P_a)(L_1 + L_2)}\cdot\left[\frac{1}{h^2} - \frac{1}{h_i^2}\right]. \qquad \{7\}$$

We are interested in how long it takes the asperities on the web to make contact with the asperities on the roller, $h = \alpha$. We further suppose that as the web and roller approach each other the asperities add no resistance to airflow. Assuming that h_i (initial air gap) is large compared to h_f (final air gap), h_i can be dropped and Eq. 7 simplifies to:

$$\Delta t = \frac{2\mu \cdot L_1^3}{(P_T - P_a)(L_1 + L_2)}\cdot\frac{1}{\alpha^2}\cdot \qquad \{8\}$$

(Rice [10] analyzed a squeeze film including the web mass, time varying groove pressure, and a non-infinite h_i. He showed that ignoring these effects have only a second-order effect on traction; they can safely be ignored.) Finally, Eq. 8 can be rewritten in terms of common variables already used to describe the roller traction problem. The correct squeeze film equation for a grooved roller is:

$$\Delta t = \frac{\mu \cdot L_W^2 L_F}{2(T/R - P_a)}\cdot\frac{1}{\alpha^2}, \qquad \{9\}$$

where Δt denotes the time for web to travel from h_i to α or the top of the asperities, α denotes the final film gap (asperity engagement height), denotes the land width, and L_F is the fraction of land area to total area of the roller:

$$L_F = \frac{L_W}{L_W + G_W}, \qquad \{10\}$$

where G_w denotes the groove width.

An important parameter in the web-to-roller traction problem is the distance (or time) it takes the web and roller to make initial contact. If the web is wrapped around the roller a shorter time than it takes to squeeze the air from the lands into the grooves, there will not be any contact. The web velocity, V_w, directly relates time and distance:

$$x = V_w \cdot t. \qquad \{11\}$$

The ratio of the time to squeeze the air into the grooves to the time the web is wrapped around the roller, θ^*, is an important dimensionless group. It is defined by:

$$\theta^* = \frac{\Delta t \cdot V_w}{R\theta}. \qquad \{12\}$$

The ratio: $\frac{\Delta t \cdot V_w}{R}$ is simply the portion of θ where there is no contact. If this ratio is equal to zero, there is no reduction in wrap angle. If this ratio is greater than or equal to unity, there is complete loss of wrap (and contact). The following relationship is used to calculate the effective wrap angle (θ_{eff}):

$$\begin{aligned} \theta_{eff} &= (1-\theta^*)\cdot\theta \qquad \text{when } \theta^* < 1 \\ \theta_{eff} &= 0 \qquad\qquad\quad \text{when } \theta^* \geq 1 \end{aligned} \qquad \{13\}$$

The effective wrap angle accounts for the loss of wrap as a result of air entrainment with grooved rollers.

Designing Rollers with Adequate Traction

The dimensionless groups P^*[1] and θ^* are very useful for roller design. Maximum traction is attained when both are equal to zero. If either ratio exceeds unity there is a complete loss of traction.

The following simple relationship should give a reasonable estimate of the effective coefficient of friction (f_e) [3, 11]:

$$f_e = \frac{F_c}{F_T}\cdot f \qquad \{14\}$$

where F_c is found by integrating the contact pressure (P_c) between the web and roller over the surface area, and the maximum available contact force (F_T) is available only when there is no air entrainment. The effective coefficient of friction represents the reduction in the normal force (F_c) as a result of air entrainment.

We use a normalized friction value termed *effective venting* (γ) to understand the effect of air entrainment on web-to-roller traction independent of f. Effective venting is defined as:

$$\gamma = \frac{f_e}{f} = \frac{F_c}{F_T} \leq 1 . \qquad \{15\}$$

Effective venting has a value of unity when there is no air entrainment and a value of zero when there is a complete loss of traction. By making the appropriate substitutions, Eq. 15 can also be written as:

$$\begin{aligned} \gamma &= (1-\theta^*)\cdot(1-P^*) \\ \gamma &= 0 \end{aligned} \quad \text{when} \quad \begin{aligned} &P^* \text{ and } \theta^* \leq 1 \\ &P^* \text{ or } \theta^* > 1 \end{aligned} \qquad \{16\}$$

The dimensionless ratio P^* denotes the ratio of the steady-state air pressure to the web tension pressure:

$$P^* = \frac{P_a}{T/R} = \frac{3.094\mu V}{T_0 - c\rho V_w^2}\left(\frac{R}{h_{eff}}\right)^{3/2} . \qquad \{17\}$$

When P^* is equal to or greater than unity, all the web tension pressure is balanced by air pressure and $P_a = T/R$. The web begins to float away from the roller surface and contact is lost. When P^* is equal to zero, there is no air entrainment and full traction is realized. To minimize the loss of traction because of the steady-state air pressure, we want to minimize R, V_w, and V_r and maximize T and h_{eff}. For grooved rollers increasing groove depth and decreasing land fraction are the most efficient ways to increase h_{eff}. For non-grooved rollers, increasing web/roller surface roughness is the only way to increase h_{eff}

The dimensionless ratio θ^* denotes the ratio of the time to squeeze the air from the lands into the grooves to the time the web is wrapped around the roller:

$$\theta^* = \frac{\Delta t \cdot V_w}{R\theta} = \frac{1}{2R\theta \cdot \alpha^2} \cdot \frac{\mu \cdot L_W^2 \cdot L_F \cdot V_w}{T/R - P_a} . \qquad \{18\}$$

This ratio represents a reduction in the nominal wrap angle. If the ratio is equal to zero, there is no reduction in wrap angle. If the ratio is greater than or equal to unity, there is complete loss of wrap (and traction). To minimize loss of wrap angle (and traction) as a result of air entrainment, we want to minimize L_w, L_F, P_a, and V_w, and maximize α, T, and θ. (The roller radius R has minimal affect on θ^*.)

The steady-state groove pressure (P_a) is easy to minimize by choosing a sufficient groove depth. It is interesting to study θ^* for the special case where $P_a = 0$:

$$\theta^* = \frac{\Delta t \cdot V_w}{R\theta} = \frac{\mu \cdot L_F \cdot V_w}{2T\theta} \cdot \frac{L_W^2}{\alpha^2} . \qquad \{19\}$$

This shows that roller radius has minimal affect on θ^*.

Improved Modified Capstan Equation

Traction testing causes the tension in the circumferential direction to vary because of frictional forces developed between the web and test roller. This must be taken into account when using a model to predict experimental measurements of web-to-roller traction. Equation 14 assumes the circumferential tension is constant. The modified capstan equation [1] accounts for varying tension in the circumferential direction account but does not account for the loss of wrap associated with circumferentially grooved rollers. This is easily remedied by substituting θ_{eff} into the modified capstan equation [1] yielding:

$$\frac{T_{high} - P_a R}{T_{low} - P_a R} = e^{f\theta_{eff}} , \qquad \{20\}$$

where $T_{high} = T_{high0} - c\rho V_w^2$, $T_{low} = T_{low0} - c\rho V_w^2$, T_{high0} denotes the high-side web tension per unit width, T_{low0} denotes the low-side web tension per unit width, c denotes the web thickness, ρ denotes the web mass-per-unit volume, V_w denotes the web speed, θ_{eff} is given by Eq. 13, and P_a is given by Eq. 2. The term P_a accounts for a loss of F_c because of super-ambient air pressure [1]. The term θ_{eff} accounts for a loss of F_c because of wrap angle loss.

Equation 20 is the capstan equation including the effects of air entrainment and centripetal acceleration (hereafter referred to as the "2D model") for non-grooved and circumferentially grooved rollers at impending slippage. Solving for T_{high}-T_{low} in Eq. 20 yields the web-to-roller traction (ΔT) when T_{high} is held fixed in the presence of an air lubricating film:

$$\Delta T = T_{high} - T_{low} = (T_{high} - P_a R)\frac{(e^{f\theta_{eff}} - 1)}{e^{f\theta_{eff}}}. \qquad \{21\}$$

EXPERIMENTAL TRACTION MEASUREMENTS AND RESULTS

The test facility is described in detail in [10] and [11]. The equivalent coefficient of friction is measured by applying a slowly increasing braking torque using a pneumatically actuated PRONY brake [12] to the test roller until slip is detected between the test roller and web. Slip is supposed to have occurred when the ratio of the time required for one revolution of the test roller to the time required for one revolution of a reference roller varies by more than 0.3% from a reference value. For the dynamic traction tester, f_e, is computed for experimental measurements as follows [11]:

$$f_e = \frac{1}{\theta}\ln\left[\frac{T_{high0}}{T_{high0} - \Delta T}\right]. \qquad \{22\}$$

Substituting Eq. 21 into Eq. 22 yields:

$$f_e = \frac{1}{\theta}\ln\left[\frac{T_{high0}}{T_{high0} - \left[(T_{high} - P_a R)\frac{(e^{f\theta_{eff}} - 1)}{e^{f\theta_{eff}}}\right]}\right]. \qquad \{23\}$$

Equation 23 allows us to compare our 2D model directly to experimental data of roller traction. The static coefficient of friction is estimated from the y intercepts of the plots of effective coefficient of friction versus speed [10]. The surface roughness parameters for the webs and roller were measured with an optical surface profiler using techniques described in Rice *et al.* [11].

Regression Analysis of the 2D Model Prediction of Traction

We traction-tested a series of 14 rollers and 19 webs. Not all possible combinations were tested; we used 373 experimental points to assess the 2D model. Table 1 provides a matrix of the web and roller combinations traction tested. Table 2 shows the minimum

and maximum range of variables tested. The maximum and minimum ranges were not investigated for all roller-web combinations listed in Table 1.

roller #	1	2	3	4	5	6	7	8	9	10	11	12	13	14
web #														
1	x													
2	x													
3	x													
4	x													
5		x	x											
6		x	x										x	
7		x	x											
8				x										
9					x	x								
10							x	x	x	x	x	x		
11							x	x	x	x	x	x		x
12					x	x								
13					x	x								
14					x	x								
15					x	x								
16					x	x								
17				x										
18				x										
19				x										

Table 1. - Test matrix.

	radius	N	G_D mean	thickness	θ	α	f	T_0
	(m)	(m^{-1})	(μm)	(μm)	(deg)	(μm)		(N/m)
minimum	0.035	0	0	98	10	0.7	0.13	44
maximum	0.156	3937	241	272	180	25.9	0.55	350

Table 2. - Variable range tested.

The webs tested had a wide range of surface coatings, which caused significant surface roughness differences between them. The webs tested had extremely uniform geometric properties that allowed uniform cross-width tension. Uniform cross-width tension was an important assumption used in deriving the 2D model. A description of each web is provided in Table 3. The roller surfaces ranged from non-grooved to circumferential grooved rollers with groove densities from approximately 1000–4000 grooves per meter. The rollers ranged in radius from 0.035– 0.156 meters. A description of each roller is provided in Table 4.

	description	thickness	density	Young's Modulus	R_{pm} mean	R_{pm} std	R_z mean	R_z std	α_w
web #		(μm)	(kg/m^3)	(Pa)	(μm)	(μm)	(μm)	(μm)	(μm)
1	PE coated paper	272	1108	4.14E+09	6.08	0.62	10.88	0.60	8.76
2	coated PET	182	1358	4.83E+09	4.99	0.62	5.74	0.66	5.64
3	coated PET	179	1358	4.83E+09	1.04	0.14	1.22	0.20	1.19
4	uncoated PET	98	1358	4.83E+09	0.61	0.30	0.72	0.32	0.71
5	coated PET	180	1358	4.83E+09	1.45	0.17	1.55	0.14	1.54
6	coated PET	125	1358	4.83E+09	1.34	0.13	1.55	0.14	1.52
7	coated PET	100	1358	4.83E+09	0.57	0.19	0.68	0.21	0.66
8	coated PET	125	1358	4.83E+09	0.76	0.04	1.39	0.03	1.11
9	coated PET	125	1358	4.83E+09	0.66	-	0.72	-	0.72
10	coated PET	125	1358	4.83E+09	0.78	0.07	1.24	0.08	1.07
11	coated PET	125	1358	4.83E+09	1.37	0.12	1.69	0.14	1.63
12	coated PET	100	1358	4.83E+09	2.56	0.21	2.79	0.21	2.77
13	coated PET	100	1358	4.83E+09	1.08	0.02	1.30	0.03	1.26
14	coated PET	100	1358	4.83E+09	0.67	0.10	0.84	0.13	0.81
15	coated PET	100	1358	4.83E+09	0.69	0.10	0.88	0.11	0.84
16	coated PET	125	1358	4.83E+09	1.18	-	1.50	-	1.43
17	coated PET	125	1358	4.83E+09	2.16	0.42	2.41	0.47	2.38
18	coated PET	125	1358	4.83E+09	0.60	0.08	0.79	0.12	0.74
19	coated PET	125	1358	4.83E+09	3.36	0.21	3.98	0.22	3.88

Webs 1-4 were 0.7 m wide. All other webs were 1.4 m wide, except web 8 was 0.7 m wide for the 350 N/m test only.

Table 3. - Web description.

	surface material	radius	N	G_D mean	G_D std	tool radius	L_F	R_{pm} mean	R_{pm} std	R_z mean	R_z std	α_r
roller #		(m)	(m^{-1})	(μm)	(μm)	(μm)		(μm)	(μm)	(μm)	(μm)	(μm)
1	aluminum hardcoat	0.050	n/a	n/a	n/a	n/a	n/a	1.44	0.12	7.67	2.09	2.61
2	tungsten carbide	0.050	n/a	n/a	n/a	n/a	n/a	17.1	1.82	35.3	1.86	25.9
3	nickel plated	0.050	3937	43	4	127	0.25	1.25	0.09	2.88	0.20	1.96
4	nickel plated	0.050	3937	36	3	127	0.31	0.23	0.07	0.63	0.15	0.38
5	aluminum hardcoat	0.035	945	108	14	254	0.61	0.33	0.08	0.94	0.19	0.54
6	aluminum hardcoat	0.035	945	100	11	254	0.62	1.35	0.23	4.49	0.51	2.29
7	aluminum hardcoat	0.035	945	51	11	254	0.71	3.35	0.46	9.97	0.56	5.58
8	aluminum hardcoat	0.035	945	51	11	254	0.71	2.25	0.22	7.32	0.79	3.81
9	aluminum hardcoat	0.035	945	51	11	254	0.71	0.37	0.11	0.97	0.26	0.60
10	aluminum hardcoat	0.035	945	184	33	254	0.54	3.01	0.51	11.79	4.65	5.25
11	aluminum hardcoat	0.035	945	184	33	254	0.54	1.41	0.16	5.03	0.93	2.42
12	aluminum hardcoat	0.035	945	184	33	254	0.54	0.44	0.37	1.00	0.47	0.69
13	aluminum hardcoat	0.156	3150	76	4	178	0.10	1.41	-	5.03	-	2.42
14	aluminum hardcoat	0.156	945	241	13	254	0.35	1.41	-	5.03	-	2.42

All rollers were 1.5 m wide.

All roughness measurements are for the land portion only, except rollers 1, 2, and 15 are total surface.

Rougness wasn't measured for rollers 13 and 14, typical values were used from similar rollers.

GD std for rollers 13 and 14 is based on typical values for rollers made with similar manufacturing processes.

Table 4. - Roller description.

Figure 4 is a plot of f_e from experimental data for the 2D model's prediction of f_e. Each experimental point in Fig. 4 is the average of 3 measurements. The average variance for these 3 repeats was 0.000177 for all experimental points (n = 373) taken. The 95% confidence limits are $\pm$ 0.027 ($\pm$2 standard deviations) on the experimental values of f_e reported. A regression analysis of the experimental data shown in Fig. 4 gives an R^2 = 0.957 with a slope of 1.008 (compared to the desired nominal value of unity).

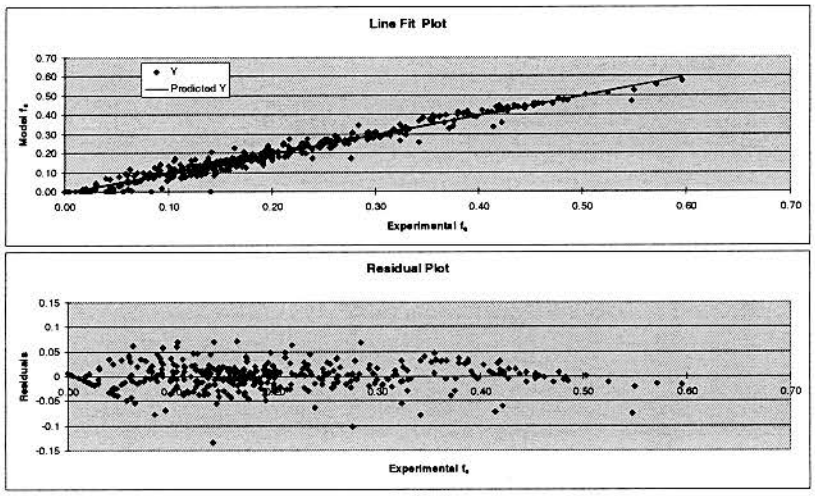

Fig. 4. - Regression analysis of model prediction of f_e.

Figure 5 is a plot of experimental data for γ versus the 2D model predictions of γ. A regression analysis of the experimental data shown in Fig. 5 has an R^2 value of 0.882 and a slope of 0.984 (compared to the desired nominal value of unity). The effective venting parameter (γ) is a more sensitive parameter than f_e to validate the 2D model. Normalizing f_e by f increases the maximum 2D model error to essentially 1.0, regardless of the actual value of f.

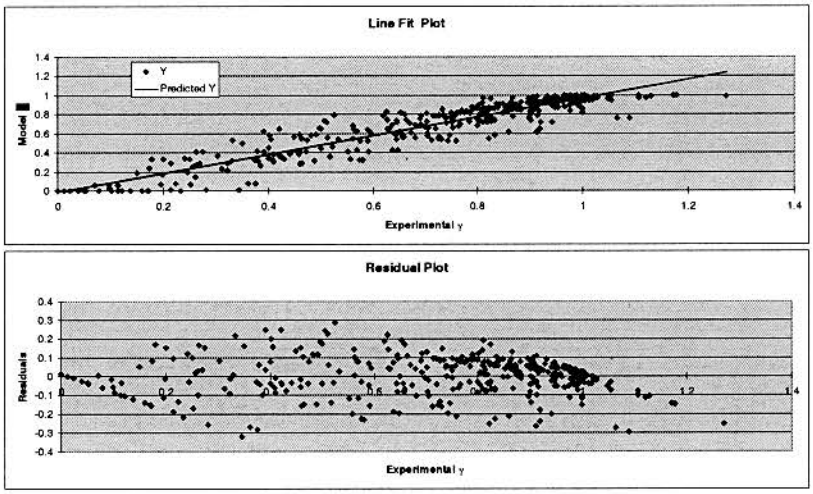

Fig. 5. - Regression analysis of model prediction of γ.

The Effect of Surface Roughness on Roller Traction

Next, a few typical experimental measurements are compared to our 2D model to illustrate the effect of surface roughness on traction for low-wrap circumferentially grooved rollers. The appropriate values for: h_{eff}, f, θ, α, T_{high0}, etc., needed for the 2D model in the following examples are given in Table 5.

roller #	web #	θ	α	f	T_0	G_{Deff}	h_{eff}
		(deg)	(μm)		(N/m)	(μm)	(μm)
5	9	93	0.9	0.17	131	85.5	62.5
5	9	10	0.9	0.14	131	85.5	62.5
6	9	93	2.4	0.32	131	79.0	57.2
6	9	10	2.4	0.30	131	79.0	57.2
8	10	11	4.0	0.23	131	39.6	26.2
9	10	11	1.2	0.18	131	39.6	26.2
11	10	11	2.7	0.18	131	149.0	115.0
12	10	11	1.2	0.19	131	149.0	115.0

μ_a =1.81e-5 N-s/m^2

p_{atm}=101e5 Pa

Table 5- Run description.

Figure 6 shows plots of f_e for course pitch grooved rollers 5 and 6 predicted by the 2D model (Eq. 23) and experimental results. The error bars on the experimental data represent 95% confidence limits of the experimental data. The groove depth (approximately 100 μm) and profile are basically identical for both rollers. The effective wrap angle (Eq. 13) for roller 5 at 5 meters per second is 3.2 and 86.6° for 9.8 and 93.2° of nominal wrap, respectively. The effective wrap angle for rough roller 6 at 5 meters per second is 8.8 and 92.2° for 9.8 and 93.2° of apparent wrap, respectively. Roller 5 looses 67 and 7% of its apparent wrap angle (tangent-to-tangent point) at 9.8 and 93.2° of wrap, respectively. This loss of wrap angle is the reason why roller 5 has such poor traction for the low-wrap angle case. The loss of wrap is much more significant for low-wrap cases because it accounts for a much larger portion of the total wrap. The loss of wrap for roller 6 is much less because of its higher surface roughness, when compared to roller 5 (α_r equal to 2.29 versus 0.54 μm, see Table 4). According to the squeeze film model, wrap angle, land width, and roughness are important in determining the effective coefficient of friction.

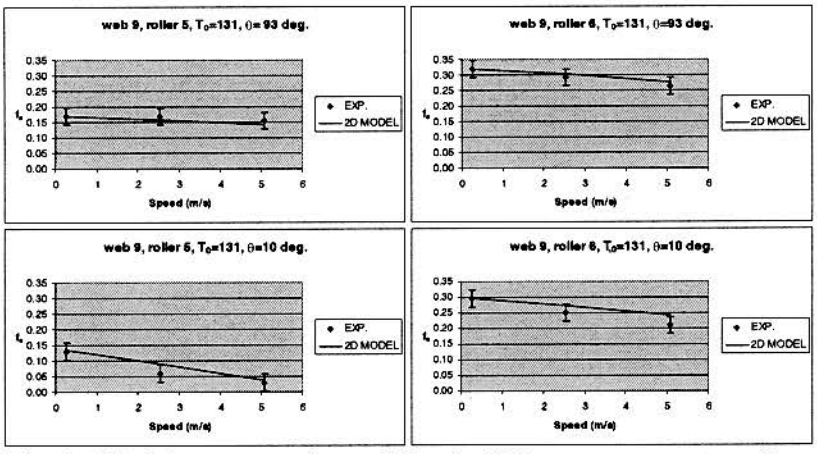

Fig. 6. - Model versus experimental data for 945 grooves per meter rollers.

Figure 7 shows a prediction of f_e using the 2D model versus experimental results for grooved rollers 8, 9, 11, and 12. Roller cross sections are shown in Fig. 8. The groove depths for rollers 9 and 12 were 51 and 184 μm, respectively. Both of these rollers have very smooth land surface roughness (α_r equal to 0.6 and 0.7 μm for rollers 9 and 12,

Rec 16 Oct 00 B

respectively). The groove depth of roller 8 is the same as roller 9; likewise, the groove depth of roller 11 is the same as roller 12. Both of these rollers have much rougher lands (α_r equal to 3.8 and 2.4 μm, respectively) than rollers 9 and 12. Looking at Fig. 7, the rougher rollers (8 and 11) are less susceptible to air entrainment than the smoother rollers (9 and 12).

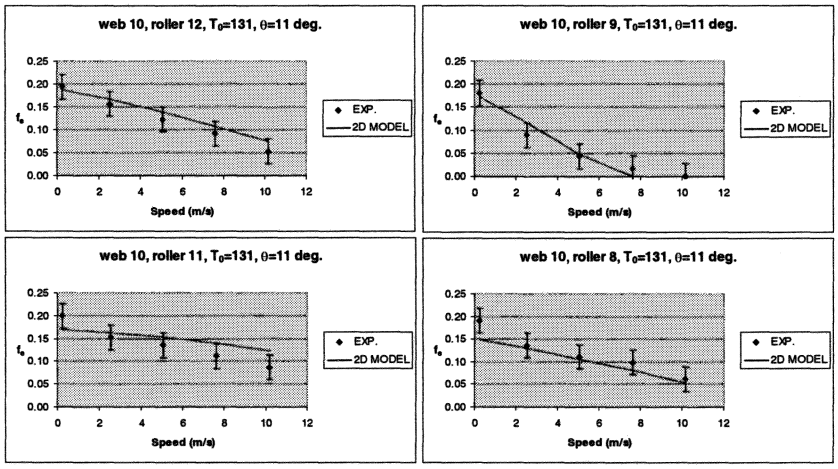

Fig. 7. - Model versus experimental data for 945 grooves per meter rollers.

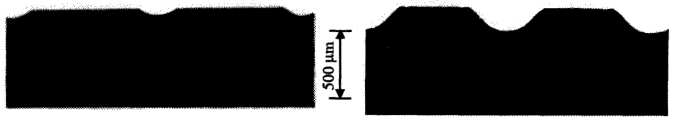

(c) roller 9 (d) roller 12

Fig. 8. - Roller groove cross sections using surface replicas: (a) roller 9; (b) roller 12.

LIMITING CONDITIONS ON THE 2D MODEL

Cross-Width Bending Stiffness

The 2D model requires the web to be rigid in the cross-width (y) direction. Rice [10] showed that when the following inequality is satisfied:

$$B^* = \frac{(T/R)(1/N)^4}{cD} < 38.4\,, \qquad \{24\}$$

where $D = \frac{Ec^3}{12(1-\nu^2)}$, the web is sufficiently rigid. None of the experiments in this paper come close to violating this constraint. When ultra thin webs and/or when coarse pitch grooved rollers are used, this constraint can be violated. Rice [10] shows that when this constraint is violated, web deformations in the cross-width direction become significant and disrupt the airflow.

Loss in θ as a Result of Bending Stiffness in the Running Direction

Bending stiffness in the circumferential direction *(x)* causes a loss in θ. The total loss of wrap angle (addition of entrance and exit nips) is given by Eshel and Elrod [13] as:

$$\Delta\theta = 2\sqrt{\frac{D}{TR^2}}\,. \qquad \{25\}$$

The presence of bending stiffness gives rise to contact forces between the web and roller, which are absent when bending stiffness is negligible. There is a line load (perpendicular to the roller surface) generated at the initial point of contact and at the last point of contact. Using Euler-Bernoulli beam theory, Müftü and Cole [14] derived the solution for the deflection w as the web approaches the roller. The plate flexural rigidity multiplied by the third derivative of w evaluated at the initial point of contact gives the magnitude of the line load because of bending stiffness:

$$F_{line} = -D\left.\frac{d^3w}{dx^3}\right|_{x=contact} = \sqrt{\frac{TD}{R^2}}\,. \qquad \{26\}$$

There are two offsetting effects caused by the bending stiffness of the web: (1) less area for the T/R pressure to act (because of loss of wrap angle), and (2) additional normal forces between the web and roller. The net effect on web-to-roller traction is negligible. The order one approximation for traction is simply $\Delta T = f \cdot F_c$. The total contact force for the case without bending is:

$$F_c = \frac{T}{R}\cdot R\theta = T\theta\,. \qquad \{27\}$$

The total contact force for the case with bending is the sum of the tension pressure force (acting over the remaining wrap angle) and the additional line load at both the entrance and exit nip:

$$F_c = \frac{T}{R}\cdot R\cdot(\theta - \Delta\theta) + 2\sqrt{\frac{TD}{R^2}} = T\left(\theta - 2\sqrt{\frac{D}{TR^2}}\right) + 2\cdot\sqrt{\frac{TD}{R^2}} = T\theta\,. \qquad \{28\}$$

The total resultant force is the same with or without bending. Because the total contact force remains unchanged, the web-to-roller traction (based on the order one solution) will be the same. This allows the 2D model to yield good results, even though the loss in wrap angle and the additional forces, due to bending, are not taken into account.

SUMMARY

We studied the traction developed between a thin, flexible web and a rotating cylindrical roller with circumferential grooves analytically and experimentally. We developed a *modified capstan equation* that includes the effect of air entrainment for both non-grooved and circumferentially grooved rollers:

$$\frac{T_{high} - P_a R}{T_{low} - P_a R} = e^{f\theta_{eff}}\,. \qquad \{29\}$$

The term $P_a R$ represents a reduction in contact force as a result of air entrainment and the term θ_{eff} represents a loss in wrap angle as a result of air entrainment. This equation extends the work of Rice and Gans [1] to arbitrary wrap angles.

We verified the modified capstan equation with 373 experimental observations of roller traction over a wide range of process and design variables. The correlation of the model with experimental data was excellent ($R^2 = 0.96$). We showed that surface roughness is important for low-wrap circumferentially grooves rollers.

It is surprising that the modified capstan equation works so well over such a large range of variables tested. The fact that it works even when some of the assumptions of the foil bearing equation are violated is curious [10]. The correlation with experimental data is not fortuitous; it correlates well for most of 373 experimental observations. However, extreme caution should be exercised when using the modified capstan equation to extrapolate outside the range of variables tested in this paper.

Simple dimensionless groups (P^* and θ^*) were derived to help the roller designer quantitatively study the interactions of process variables (e.g., speed and tension) with design variables (e.g., groove depth, groove pitch, roughness, etc.). The utility of the dimensionless ratios and the modified capstan equation is based on their simplicity. No FD or FE codes are needed—just a pencil and a piece of paper. These equations should have broad applications in many research disciplines. Examples include: wear of the head/tape interface, torque capacity of thin belts, etc.

REFERENCES

1. Rice, B. S. and Gans, R. F., 2003, "A Simple Model to Predict Web-to-Roller Traction," *Proc. Seventh Int. Web Handling Conf.,* Oklahoma State University, Stillwater, OK, June.
2. Hourticolon, R., Roth, G., Frenken, H., Schäffer, H., and Koepke, G., 1984, "Web Guide Roller for Use at High Speeds and Process for Producing the Same," U. S. Patent No. 4,426,757.
3. Ducotey, K. S. and Good, J. K., 2000, "A Numerical Algorithm for Determining the Traction Between a Web and a Circumferentially Grooved Roller," *Trans. ASME, J. Tribology*, 122, pp. 578–584.
4. Smith, D. P. and Von Behren, R. A., 1989, "Squeeze film Analysis of Tape Winding Effects in Data Cartridge," *Tribology and Mechanics of Magnetic Storage Systems*, STLE-SP-26, pp. 88–92.
5. Keshavan, M. B. and Wickert, J. A., 1997, "Air Entrainment During Steady State Web Winding," *Trans. ASME, J. of Applied Mechanics*, 64, pp. 916–922.
6. Ducotey, K. S. and Good, J. K., 1998, "The Effect of Web Permeability and Side Leakage on the Air Film Height Between a Roller and Web," *Trans. ASME, J. Tribology*, 120, pp. 559–565.
7. Ducotey, K. S. and Good, J. K., 1999, "Predicting Traction in Web Handling," *Trans. ASME, J. Tribology*, 121, pp. 1–7.
8. Hashimoto, H., L., 1999, "Air Film Thickness Estimation in Web Handling Processes," *Trans. ASME J. Tribology*, Vol. 121, pp.50–55.
9. Hamrock, B. J., 1994, *Fundamentals of Fluid Film Lubrication*, McGraw-Hill, NY.
10. Rice, B. S., 2003, *Reduction in Web-to-Roller Traction as a Result of Air Lubrication*, Ph.D. thesis, University of Rochester, Rochester, NY.
11. Rice, B. S., Müftü, S., and Cole, K. A., 2002, "A Model for Determining the Asperity Engagement Height in Relation to Web Traction over Non-vented Rollers," *Trans. ASME, J. Tribology*, Vol. 124, pp. 584–594.

12. Oberg, E. Jones, F. D. and Horton, H. L., 1980, *Machinery's Handbook 23rd Edition*, Industrial Press, New York, NY.
13. Eshel, A. and Elrod, H. G. Jr., 1967, "Stiffness Effects on the Infinitely Wide Foil Bearing," *ASME J. Basic Eng.*, Dec., pp. 831–836.
14. Müftü, S. and Cole, K. A., 1999, "The Fluid/Structure Interaction in Supporting a Thin Flexible Cylindrical Web With an Air Cushion," *J. Fluids Struct.*, 13, pp. 681–708.